Analysis of a Discrete Spectrum Analyzer for the Detection of Radio Frequency Interference

B. K. Levitt
Communications Systems Research Section

As the radio frequency spectrum becomes increasingly overcrowded, interference with mission-critical DSN operations is rising at an alarming rate. To alleviate this problem the DSN is developing a wideband surveillance system for on-site detection and identification of potential sources of radio frequency interference (RFI), which will complement the existing frequency coordination activities. The RFI monitoring system is based on a wideband, multi-look discrete spectrum analyzer operating on fast Fourier transform principles. This article presents an extensive general statistical analysis of such spectrum analyzers and derives threshold detection performance formulas for signals of interest. These results are then applied to the design of the RFI spectrum analyzer under development.

I. Introduction

Due to the steady increase of commercial and military users of the radio frequency (RF) spectrum, deep space telemetry and tracking can no longer expect to have dedicated, interference-free bands available all the time. DSN operations are particularly vulnerable to radio frequency interference (RFI) because of the relatively weak signals received from deep space probes. The magnitude of this problem was addressed in part by an earlier article (Ref. 1), which demonstrated the potential for an alarming number of outages in DSN reception due to RFI from a rapidly growing contingent of powerful Earth-orbiting satellites.

To alleviate this problem, the DSN is developing equipment to provide continuous, real-time surveillance of the RF environment at each complex. This monitoring system will function independent of existing DSS receivers and antennas so as to avoid interrupting normal DSN operations. By detecting and identifying potential sources of RFI in advance, and using available frequency coordination procedures, the loss of mission-critical data can be minimized.

The heart of the RFI monitoring system under development is a wideband (10-20 MHz at S-band), high-resolution (2^{17}, or about 130,000 spectral lines), digital spectrum analyzer, using fast Fourier transform (FFT) processing for real-time operation. This article determines the statistical performance of discrete spectrum analyzers corrupted by additive Gaussian noise, and applies the resulting formulas to the design of the RFI surveillance system.

Much of the detailed mathematical analysis is confined to a series of appendices. A general expression for the power in a

given spectral line is derived in Appendix A for a discrete Fourier transform (DFT) spectrum analyzer. (The FFT is simply a computationally efficient method of implementing a DFT). This is followed by an examination of the statistical characteristics of the spectral line powers for an "L-look" analyzer (in which the output powers are averages of L independent measurements), and the derivation of system performance probabilities for threshold signal-detection processing. In Appendix B, this is done for continuous spectrum bandpass Gaussian signals, while Appendix C looks at discrete spectrum signals imbedded in white Gaussian noise. Finally, Appendix D discusses aliasing effects in the DFT spectrum resulting from the finite observation window for the input signal.

II. Application to RFI Spectrum Analyzer Design

In this section, we will use some of the statistical performance formulas derived in the appendices to compute some preliminary design parameters for the RFI spectrum analyzer. This is an L-look, FFT-based system which produces an $N = 2^{17}$ line spectrum of total bandwidth $W = 10$ MHz (baseline design), so that the line width is $W/N = 76.3$ Hz. The system internal noise temperature is assumed to be 30 K in this exercise, corresponding to a thermal noise power spectral density $N_0 = -183.83$ dBm/Hz.

For RFI applications, most of the time the spectrum analyzer will see only its own thermal noise. In this case, Appendix B shows that each of the normalized spectral line powers is a central chi-square random variable with $2L$ degrees of freedom, mean 1, and standard deviation $1/\sqrt{L}$ (see Eq. B-16 with signal-to-noise ratio $\gamma = 0$). If a threshold $\eta > 1$ is used to detect the presence of an external signal component at each line frequency, the false alarm probability per line P_{FA} is given by Eq. (B-21). Since it requires T_L seconds (see Eq. B-12) to generate one entire spectrum, the probability of a false alarm on any line during 24 hours of continuous operation, $P_{FA}{}^*$, is overbounded by

$$P_{FA}{}^* < \frac{(24 \times 60 \times 60)N}{T_L} P_{FA} < \frac{86400W \left[\eta e^{-(\eta-1)}\right]^L}{\sqrt{2\pi L}\,[(\eta-1)L+1]} \tag{1}$$

which is accurate for small $P_{FA}{}^*$ (union bound argument) and $(\eta-1)\sqrt{L} \gtrsim 4$ (see Fig. B-3).[1] For reliable RFI surveillance on a round-the-clock basis, we will arbitrarily set a baseline design requirement that $P_{FA}{}^* = 10^{-3}$. The variation of L and T_L with η subject to this constraint is illustrated in Fig. 1; note that $(\eta-1)\sqrt{L}$ varies slowly over the range of η shown.

Occasionally, the RFI spectrum analyzer will receive an external signal of interest. The Consultative Committee for International Radio (CCIR) Recommendation 365-2 states that the interference from any RFI source, measured at the input to a DSN receiver, shall not exceed -190 dBm/Hz (7.25 K) for more than 5 minutes each day. As in our first RFI article (Ref. 1), we shall assume that this power spectral density is the minimum RFI level of interest, and design the spectrum analyzer to detect signals down to this level.

The interference signal spectrum can have many forms. Suppose the sidebands from a wideband (e.g., spread-spectrum) transmission lie in the DSN receive band. Then the RFI signal might look like white Gaussian noise, with one-sided power spectral density N_0' over the spectrum analyzer bandwidth W. This situation is considered in Appendix B. The probability P_M that a given spectral line power lies below the detection threshold η, referred to as a "miss," is accurately approximated by Eq. (B-20) for large L. The tradeoff between P_M and $P_{FA}{}^*$ vs η is illustrated in Fig. 2 for $L = 2100$ and $N_0' = -190$ dBm/Hz. If we select for our baseline design the balanced performance requirement $P_M = P_{FA}{}^* = 10^{-3}$, this is satisfied for the above N_0' by the system parameters

$$\begin{gathered} L = 2091 \text{ and } \eta - 1 = 0.1587 \\ \Downarrow \\ T_L = 27.4 \text{ s and } (\eta - 1)\sqrt{L} = 7.26 \end{gathered} \tag{2}$$

For this design, the sensitivity of P_M to changes in N_0' is shown in Fig. 3 ($P_{FA}{}^*$ remains constant at 10^{-3}, of course, independent of N_0').

On the other hand, the interfering source might transmit a discrete, higher-order carrier or subcarrier harmonic component that falls into the DSN receive band. For example, suppose the RFI signal is a single sinusoid of power P at some frequency f_s, where f_s is a priori uniformly distributed over the spectrum analyzer bandwidth W. This is a special case of the M-sinusoid analysis in Appendix C. Consider the spectral line *nearest* in frequency to f_s, and denote this frequency separation by Δ: then Δ is uniformly distributed over $(-W/2N, W/2N)$. To properly detect the RFI signal, we want this particular spectral line power to be above the threshold η. Conditioned on Δ, the probability of this not occurring (a

[1] Note that the threshold is $(\eta-1)\sqrt{L}$ standard deviations beyond the mean normalized spectral line power in the noise-only case.

miss) is given by Eqs. (C-19) and (C-20), and (see Eq. C-17 with $M = 1$)

$$\lambda_k = \left(\frac{PN}{N_0 W}\right)\left(\frac{\sin N\Delta}{N \sin\Delta}\right)^2 \tag{3}$$

Averaging over Δ, the probability of a miss on this particular line is

$$P_M = \frac{2N}{W}\int_0^{\frac{W}{2N}} d\Delta \int_0^{\eta} dx\, e^{g_k(x)} \tag{4}$$

where $g_k(x)$ is defined by Eqs. (3) and (C-20). Since $N_0' W/N = -171.2$ dBm for the design point N_0' previously used, we will plan on a minimum detectable P in this vicinity. Thus, for $P = -170$ dBm and $T_L = 65.0$ s, the tradeoff between P_M and P_{FA}* as η is varied is shown in Fig. 4. To ensure that $P_M = P_{FA}^* = 10^{-3}$ for this P, we need

$$\begin{aligned} &T_L = 64.0 \text{ s and } \eta - 1 = 0.1003 \\ &\Downarrow \\ &L = 4883 \text{ and } (\eta - 1)\sqrt{L} = 7.01 \end{aligned} \tag{5}$$

The corresponding sensitivity of P_M to changes in P is illustrated in Fig. 5.

The design parameters of Eq. (5) represent a good baseline to cover both types of RFI signals above with their corresponding minimum detectable levels. When this selection is made, and the white noise-like RFI signals with $N_0' = -190$ dBm/Hz is present, Eq. (B-20) yields $P_M = 7.03 \times 10^{-17}$, while P_{FA}* remains at 10^{-3}.

III. Conclusions

This article presented an extensive statistical analysis of a multi-look discrete spectrum analyzer based on DFT or FFT techniques. We demonstrated that the output spectral line powers are central or noncentral chi-square random variables with many degrees of freedom for continuous spectrum Gaussian signals or discrete spectrum sinusoidal components imbedded in internal Gaussian noise. We derived threshold detection probabilities for these signals, and determined accurate simple approximations for these probabilities.

These results were applied to the design of a 10 MHz, 2^{17} line FFT spectrum analyzer with a 30 K internal noise temperature, which forms the basis for an RFI surveillance system under development for the DSN. It was shown that reliable performance down to required signal detection levels can be achieved with an approximately 5000-look system, a spectrum generation time of about a minute, and a detection threshold placed 7 standard deviations beyond the mean, noise-only spectral line power.

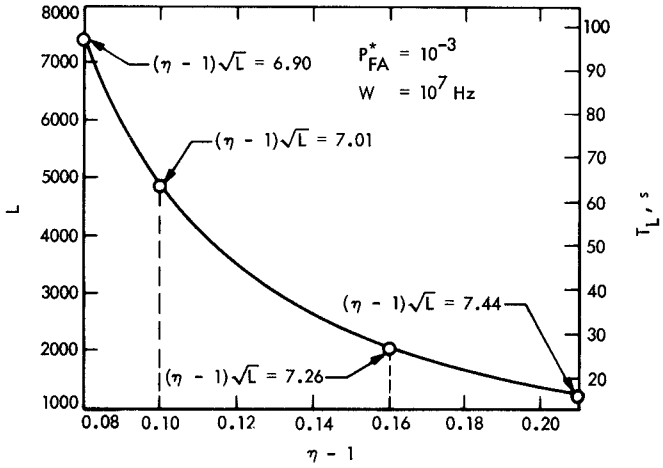

Fig. 1. Variation of number of looks L and spectrum generation time T_L with threshold η for W = 10 MHz DFT spectrum analyzer, subject to constraint that false alarm probability P_{FA}^* during 24 hours of continuous operation be 10^{-3}

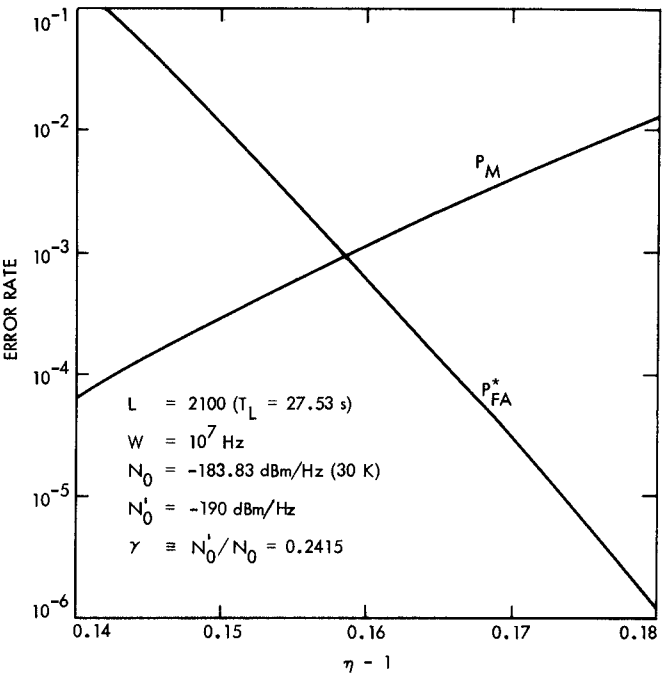

Fig. 2. Tradeoff between probability of false alarm per day P_{FA}^* and probability of a miss P_M vs threshold η for 2100-look system with spectrally white external Gaussian signal of power spectral density N'_0 = −190 dBm/Hz imbedded in internal thermal noise of power spectral density N_0 = −183.83 dBm/Hz (30 K noise temperature)

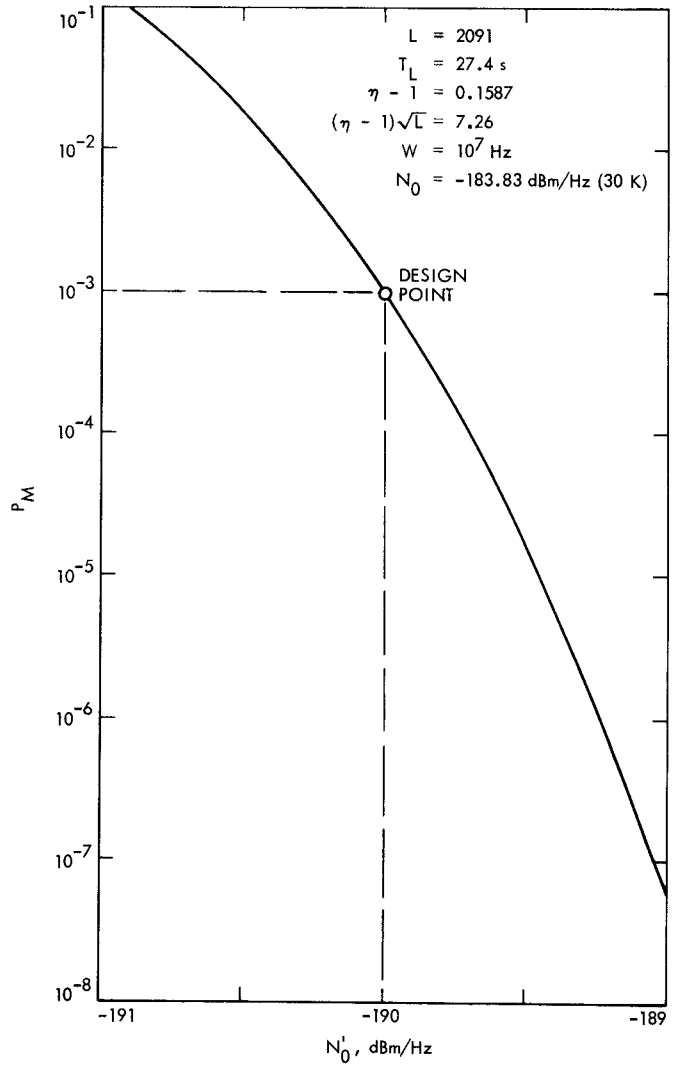

Fig. 3. Signal detection performance vs received signal power spectral density N'_0, for values of L and η selected to set $P_M = P_{FA}^* = 10^{-3}$ when $N'_0 = -190$ dBm/Hz

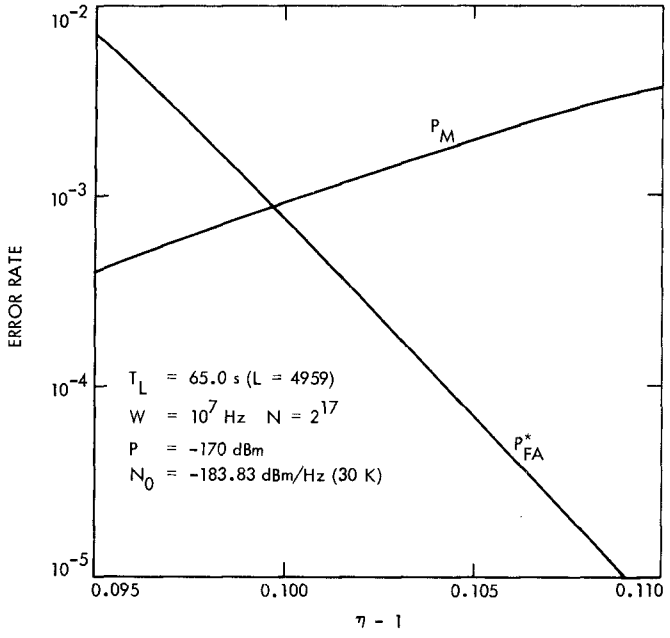

Fig. 4. DFT spectrum analyzer performance tradeoff for 65.0 s observation (4959 looks) of sinusoidal signal with power P = −170 dBm, and frequency uniformly distributed over spectral line width W/N

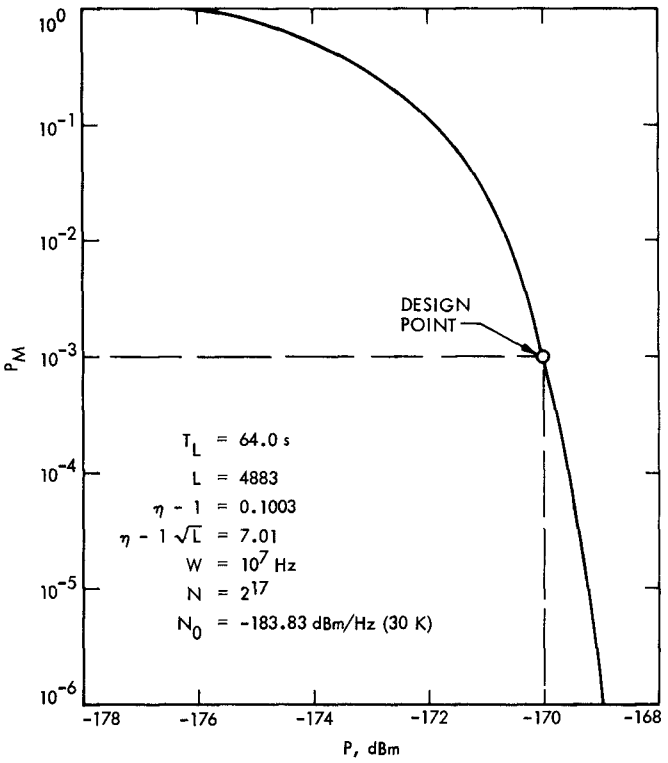

Fig. 5. Variation of probability of a miss P_M vs RFI signal power P, for values of T_L and η selected to have $P_M = P_{FA}^* = 10^{-3}$ at P = −170 dBm

Appendix A

Derivation of DFT Power Spectrum for Bandpass Signals

Consider a deterministic signal $x(t)$ with bandwidth W centered at f_c. Based on the observation of $x(t)$ over [0,T], we want to measure its power spectrum using DFT techniques.

First, $x(t)$ is reduced in quadrature to baseband, using a lowpass filter (LPF) to eliminate components near $2f_c$:

$$y(t) \equiv x(t)\ \sqrt{2}\ \text{cqs}\ 2\pi f_c t \Big|_{LPF}$$
$$z(t) \equiv x(t)\ \sqrt{2}\ \sin\ 2\pi f_c t \Big|_{LPF} \tag{A-1}$$

In the frequency domain, the corresponding Fourier transform relations are

$$Y(f) = \frac{1}{\sqrt{2}}\ [X(f-f_c) + X(f+f_c)]\Big|_{LPF}$$
$$Z(f) = \frac{1}{j\sqrt{2}}[X(f-f_c) - X(f+f_c)]\Big|_{LPF} \tag{A-2}$$

Solving for $X(f+f_c)$, we have

$$X(f+f_c) = \frac{1}{\sqrt{2}}[Y(f) - jZ(f)];\ |f| < \frac{W}{2} \tag{A-3}$$

To apply the DFT approach to the determination of $Y(f)$ and $Z(f)$, it is convenient to introduce some shorthand notation:

$$\left.\begin{aligned} y_m &\equiv y\left(\frac{m}{W}\right) \\ z_m &\equiv z\left(\frac{m}{W}\right) \end{aligned}\right\}\ m = 0,1,\ldots,N-1; N = WT$$

$$\left.\begin{aligned} Y_k &\equiv Y\left(\frac{kW}{N}\right) \\ Z_k &\equiv Z\left(\frac{kW}{N}\right) \end{aligned}\right\}\ k = -\frac{N}{2}, -\frac{N}{2}+1,\ldots,\frac{N}{2}-1, \text{for even } N \tag{A-4}$$

$$c_{km} \equiv \cos\left(\frac{2\pi km}{N}\right)$$

$$d_{km} \equiv \sin\left(\frac{2\pi km}{N}\right)$$

Then, for sufficiently large T (or equivalently, N), we have the approximation

$$Y_k \cong \int_0^T dt\, y(t)\, e^{-j2\pi kWt/N} \cong \frac{1}{W}\sum_{m=0}^{N-1} y_m(c_{km} - jd_{km}) \tag{A-5}$$

and Z_k is expressed similarly. Therefore

$$X\left(f_c + \frac{kW}{N}\right) \cong \frac{1}{W\sqrt{2}}\sum_{m=0}^{N-1}(y_m - jz_m)(c_{km} - jd_{km})$$
$$= \frac{N}{W\sqrt{2}}(A_k - jB_k) \tag{A-6}$$

where

$$A_k \equiv \frac{1}{N}\sum_{m=0}^{N-1}(y_m c_{km} - z_m d_{km})$$
$$B_k \equiv \frac{1}{N}\sum_{m=0}^{N-1}(y_m d_{km} + z_m c_{km}) \tag{A-7}$$

The one-sided power spectral density of $x(t)$ is approximated by

$$S_x(f) \cong \frac{2}{T}\left|X(f)\right|^2 \tag{A-8}$$

It follows that the k^{th} discrete power spectral component, which approximates the power in $x(t)$ with a bandwidth W/N centered at frequency $f_c + kW/N$,[2] can be expressed as

$$\frac{W}{N}S_x\left(f_c + \frac{kW}{N}\right) \cong A_k^2 + B_k^2 \equiv S_k \tag{A-9}$$

Although Eq. (A-9) was derived for deterministic signals $x(t)$, the DFT spectrum approach is readily extended to random signals, except that S_k is now a random variable, sometimes called a periodogram (Ref. 3).

[2] Actually, the finite observation time T causes some spectral spreading (see Appendix D), which can be reduced by appropriate data sample "windowing" (e.g., Refs. 2, 3).

Appendix B

DFT Power Spectrum Statistics for Continuous Spectrum Gaussian Signals

Suppose that $x(t)$ in Appendix A consists of a zero mean, bandpass, spectrally nonwhite Gaussian signal, plus zero mean, bandpass, white Gaussian noise:

$$x(t) = x_c(t)\sqrt{2}\cos 2\pi f_c t + x_s(t)\sqrt{2}\sin 2\pi f_c t \qquad \text{(B-1)}$$

where $x_c(t)$ and $x_s(t)$ are lowpass signal-plus-noise quadrature components, each with one-sided bandwidth $W/2$. If the one-sided power spectral density of $x(t)$ is $S_x(f)$, then the auto- and crosscorrelation functions of $x_c(t)$ and $x_s(t)$ can be expressed as (Ref. 4, pp. 498-501):

$$R_c(\tau) \equiv \overline{x_c(t+\tau)x_c(t)} = R_s(\tau) = \int_0^{\frac{W}{2}} df\, S_e(f)\cos 2\pi f\tau \qquad \text{(B-2)}$$

and

$$R_{cs}(\tau) \equiv \overline{x_c(t+\tau)x_s(t)} = -R_{cs}(-\tau) = -R_{sc}(\tau) = \int_0^{\frac{W}{2}} df\, S_0(f)\sin 2\pi f\tau \qquad \text{(B-3)}$$

where $S_e(f)$ and $S_0(f)$ are the even and odd parts of $S_x(f+f_c)$ about $f = 0$ (see Fig. B-1):

$$S_e(f) \equiv \frac{1}{2}[S_x(f+f_c) + S_x(-f+f_c)]$$
$$S_0(f) \equiv \frac{1}{2}[-S_x(f+f_c) + S_x(-f+f_c)] \qquad \text{(B-4)}$$

Now, to determine the spectral line statistics, we first note that the lowpass quadrature components of Eq. (A-1) are simply

$$y(t) = x_c(t) \qquad z(t) = x_s(t) \qquad \text{(B-5)}$$

Since $x_c(t)$ and $x_s(t)$ are zero mean, jointly Gaussian random processes, the spectral components A_k and B_k of Eq. (A-7) must be zero mean, jointly Gaussian random variables. Furthermore,

$$\overline{A_k^2} = \frac{1}{N^2}\sum_{m=0}^{N-1}\sum_{j=0}^{N-1} \overbrace{y_m y_j}^{R_c\left(\frac{m-j}{W}\right)} c_{km}c_{kj} + \overbrace{z_m z_j}^{R_s\left(\frac{m-j}{W}\right)} d_{km}d_{kj}$$

$$- \overbrace{y_m z_j}^{R_{cs}\left(\frac{m-j}{W}\right)} c_{km}d_{kj} - \overbrace{y_j z_m}^{R_{cs}\left(\frac{j-m}{W}\right)} c_{kj}d_{km}$$

$$= \frac{1}{N^2}\sum_{m=0}^{N-1}\sum_{j=0}^{N-1}\left[R_c\left(\frac{m-j}{W}\right)\cos 2\pi k\left(\frac{m-j}{N}\right) + R_{cs}\left(\frac{m-j}{W}\right)\sin 2\pi k\left(\frac{m-j}{N}\right)\right]$$

$$= \frac{R_c(0)}{N} + \frac{2}{N^2}\sum_{i=1}^{N-1}(N-i)\left[R_c\left(\frac{i}{W}\right)\cos\left(\frac{2\pi ki}{N}\right) + R_{cs}\left(\frac{i}{W}\right)\sin\left(\frac{2\pi ki}{N}\right)\right] = \overline{B_k^2} \qquad \text{(B-6)}$$

and similarly

$$\overline{A_k B_k} = \frac{1}{N^2}\sum_{m=0}^{N-1}\sum_{j=0}^{N-1}\left[-R_c\left(\frac{m-j}{W}\right)\sin 2\pi k\left(\frac{m-j}{N}\right) + R_{cs}\left(\frac{m-j}{W}\right)\cos 2\pi k\left(\frac{m-j}{N}\right)\right] = 0 \qquad \text{(B-7)}$$

The summation in Eq. (B-7) is zero since $R_c[(m-j)/W]$ and $\cos 2\pi k[(m-j)/N]$ are even functions of m-j, while $R_{cs}[(m-j)/W]$ and $\sin 2\pi k[(m-j)/N]$ are odd. So A_k and B_k are

independent and identically distributed. Consequently, for a single-look system, the power spectral components S_k, defined in Eq. (A-9), are central chi-square random variables with 2 degrees of freedom, and mean

$$\overline{S_k} = 2\overline{A_k^2} \tag{B-8}$$

Let us now specialize to the case where the input Gaussian signal is white, with one-sided power spectral density N_0'. If the additive noise is independent of the input signal, and has spectral density N_0 over the bandpass region of interest, we have

$$\begin{aligned} S_e(f) &= S_x(f+f_c) = N_0 + N_0';\ 0 \leqslant f \leqslant \frac{W}{2} \\ S_0(f) &= 0,\ \forall f \end{aligned} \tag{B-9}$$

Then Eqs. (B-2) and (B-3) yield

$$\begin{aligned} R_c\left(\frac{i}{W}\right) &= \frac{(N_0 + N_0')W}{2}\left(\frac{\sin \pi i}{\pi i}\right) = \frac{(N_0 + N_0')W}{2}\,\delta_{i0} \\ R_{cs}\left(\frac{i}{W}\right) &= 0,\ \forall i \end{aligned} \tag{B-10}$$

and Eqs. (B-6) and (B-8) reduce to

$$\overline{S_k} = (N_0 + N_0')\,\frac{W}{N},\ \forall k \tag{B-11}$$

where W/N is the bandwidth of a spectral line.

For an L-look DFT spectrum analyzer, the k^{th} spectral component S_k^* is the average of L independent samples of S_k, which preserves the mean and reduces the variance by $1/L$. If the L measurements are made sequentially, the total observation time is (see Eq. A-4)

$$T_L = LT = \frac{LN}{W} \tag{B-12}$$

For convenience, we will scale the entire spectrum by $(N_0 W/N)^{-1}$, so that the mean spectral line power is 1 in the absence of an input signal:

$$v_k \equiv \frac{N}{N_0 W}\,S_k^* \tag{B-13}$$

Then the normalized spectral line power v_k is a central chi-square random variable with $2L$ degrees of freedom; its probability density function is (Ref. 5)

$$p(v_k) = \frac{1}{\Gamma(L)}\left(\frac{L}{1+\gamma}\right)^L v_k^{\,L-1}\, e^{-\frac{L v_k}{1+\gamma}};\ v_k > 0 \tag{B-14}$$

where we have introduced the signal-to-noise ratio

$$\gamma \equiv \frac{N_0'}{N_0} \tag{B-15}$$

and

$$\begin{aligned} \overline{v_k} &= 1 + \gamma \\ \sigma_{v_k} &= \frac{1+\gamma}{\sqrt{L}} \end{aligned} \tag{B-16}$$

In this particular case, the input signal spectrum is flat, so the v_k's all have the same mean. However, in general, we detect the presence of a signal component at each frequency $f_c + kW/N$ by comparing v_k with a threshold η. The selection of η involves a tradeoff between the probability of incorrectly deciding a signal is not present (a "miss"), vs the probability of falsely detecting a signal (a "false alarm"): a smaller η improves the former at the expense of the latter.

The probability of a miss at the k^{th} frequency is given by (using Ref. 6, pp. 317 and 940)

$$\begin{aligned} P_M \equiv Pr\,[v_k < \eta] &= \frac{L^L}{\Gamma(L)} \int_0^{\frac{\eta}{1+\gamma}} dx\, x^{L-1}\, e^{-Lx} \\ &= e^{-\frac{\eta L}{1+\gamma}} \sum_{i=L}^{\infty} \frac{\left(\frac{\eta L}{1+\gamma}\right)^i}{i!};\ \forall k \end{aligned} \tag{B-17}$$

To ensure an acceptable balance between the miss and false alarm error rates, we select an η in the range $(1, 1+\gamma)$. Therefore the terms in the summation of Eq. (B-17) decrease mono-

tonically with i over the range $i \geq L$, suggesting the expansion (similar to Ref. 7):

$$P_M = \frac{1}{L!} e^{-\frac{\eta L}{1+\gamma}} \left(\frac{\eta L}{1+\gamma}\right)^L \left\{1 + \frac{\left(\frac{\eta L}{1+\gamma}\right)}{L+1} + \frac{\left(\frac{\eta L}{1+\gamma}\right)^2}{(L+1)(L+2)} + \cdots\right\}$$

$$< \frac{1}{L!} e^{-\frac{\eta L}{1+\gamma}} \left(\frac{\eta L}{1+\gamma}\right)^L \sum_{i=0}^{\infty} \left[\frac{\eta L}{(1+\gamma)(L+1)}\right]^i$$

$$= \frac{\left[\left(\frac{\eta L}{1+\gamma}\right) e^{-\frac{\eta}{1+\gamma}}\right]^L}{L!\left[1 - \frac{\eta L}{(1+\gamma)(L+1)}\right]} \qquad \text{(B-18)}$$

The upperbound in Eq. (B-18) becomes tight for large values of L, as will be shown later for a similar upperbound to the false alarm probability. Furthermore, $L!$ is bounded by (Ref. 8, p. 257):

$$\sqrt{2\pi L}\,(L/e)^L \leq L! \leq \sqrt{2\pi L}\,(L/e)^L\, e^{\frac{1}{12L}} \qquad \text{(B-19)}$$

and the lowerbound on $L!$ (called Stirling's approximation) is also accurate for large L (*e.g.*, within 1% for $L > 8$, and 0.1% for $L > 83$). Combining Eqs. (B-18) and (B-19) yields the useful approximation

$$P_M < \frac{\left[\left(\frac{\eta}{1+\gamma}\right) e^{1-\frac{\eta}{1+\gamma}}\right]^L}{\sqrt{2\pi L}\left[1 - \frac{\eta L}{(1+\gamma)(L+1)}\right]} \qquad \text{(B-20)}$$

The false alarm probability for a given spectral line is similarly expressed as

$$P_{FA} \equiv P_r\,[v_k > \eta \mid \gamma = 0] = e^{-\eta L} \sum_{i=0}^{L-1} \frac{(\eta L)^i}{i!}$$

$$< \sqrt{\frac{L}{2\pi}}\, \frac{\left[\eta e^{-(\eta-1)}\right]^L}{(\eta-1)L+1}\,; \forall k \qquad \text{(B-21)}$$

Another common approach to approximating the false alarm rate for large L is based on the central limit theorem (CLT):

$$p(v_k \mid \gamma = 0) \cong \sqrt{\frac{L}{2\pi}}\, e^{-\frac{L(v_k-1)^2}{2}} \qquad \text{(B-22)}$$

$$\Downarrow$$

$$P_{FA} \cong Q\left[(\eta - 1)\sqrt{L}\right] \qquad \text{(B-23)}$$

where

$$Q(\beta) \equiv \frac{1}{\sqrt{2\pi}} \int_{\beta}^{\infty} dx\, e^{-\frac{x^2}{2}} \qquad \text{(B-24)}$$

is the Gaussian error function (Ref. 4, pp. 82-83). Note that $(\eta-1)\sqrt{L}$ is $(\eta-\bar{v}_k)/\sigma_{v_k}$ conditioned on $\gamma = 0$; the larger this parameter is, the further the threshold η is into the tail of $p(v_k|\gamma = 0)$. Since the CLT approximation is only accurate near the mean, Eq. (B-23) is only useful for small $(\eta-1)\sqrt{L}$. Also, since the Gaussian probability distribution tail dies faster than the actual chi-square tail, the CLT false alarm approximation is actually a lowerbound, except for very small values of $(\eta-1)\sqrt{L}$. These comments are reinforced quantitatively in Fig. B-2.

The two false alarm approximations are compared in Fig. B-3. We see that Eq. (B-21) is accurate for $(\eta-1)\sqrt{L} \gtrsim 4$ independent of L itself, while Eq. (B-23) is only valid for $(\eta-1)\sqrt{L} \lesssim 2$ and very large $L \gtrsim 1000$.

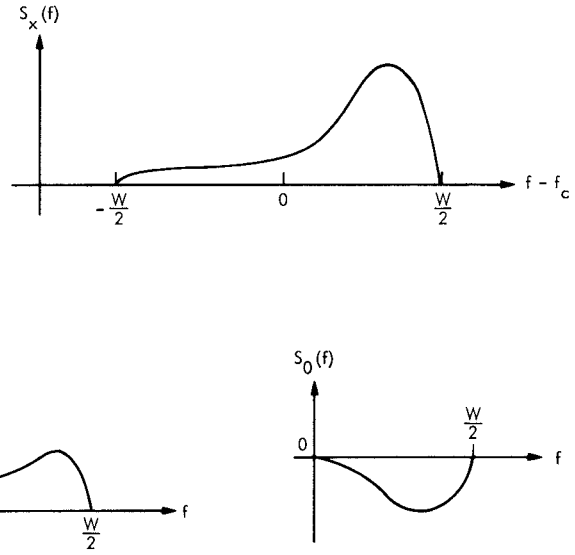

Fig. B-1. One-sided power spectral density $S_x(f)$ of colored bandpass signal $x(f)$. $S_e(f)$ and $S_0(f)$ are the even and odd parts of $S_x(f)$ about $f = 0$, for $0 \leq f \leq W/2$

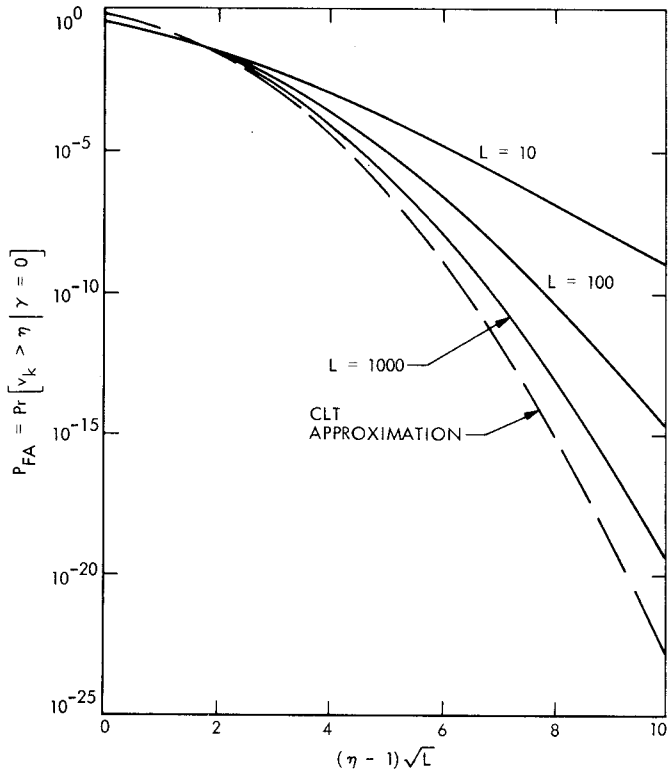

Fig. B-2. Accuracy of central limit theorem (CLT) approximation for false alarm probability P_{FA}, where v_k is a central chi-square random variable with $2L$ degrees of freedom, and $\overline{v_k} = 1$, $\sigma_{v_k} = 1/\sqrt{L}$

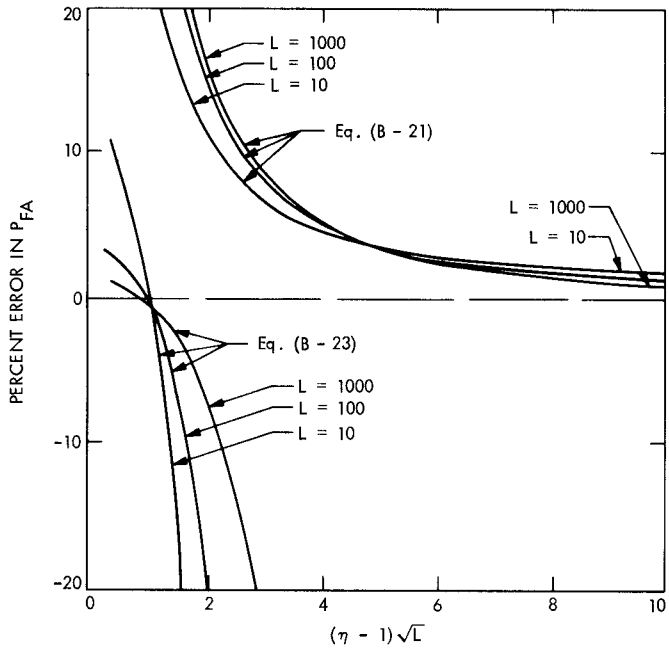

Fig. B-3. Comparison of two false alarm approximations with actual value

Appendix C

DFT Power Spectrum Statistics for Discrete Spectrum Signals

Now let $x(t)$ consist of a sum of M sinusoidal components, with the i^{th} one having power P_i, frequency $f_i \epsilon [f_c - (W/2), f_c + (W/2)]$, and phase θ_i, plus bandpass, white Gaussian noise:

$$x(t) = \sum_{i=1}^{M} \sqrt{2P_i} \sin(2\pi f_i t + \theta_i) + \sqrt{2}\,[n_c(t)\cos 2\pi f_c t + n_s(t)\sin 2\pi f_c t] \tag{C-1}$$

The lowpass noise terms $n_c(t)$ and $n_s(t)$ are independent, zero mean, jointly Gaussian random processes (Ref. 4, Eq. 7.28), each with one-sided power spectral density N_0 over $0 \leq f \leq (W/2)$, and autocorrelation function

$$R_n(\tau) = \frac{N_0 W}{2}\left(\frac{\sin \pi W\tau}{\pi W\tau}\right) \tag{C-2}$$

The lowpass quadrature components of $x(t)$ are (see eq. A-1):

$$y(t) = \sum_{i=1}^{M} \sqrt{P_i} \sin[2\pi(f_i - f_c)t + \theta_i] + n_c(t)$$
$$z(t) = \sum_{i=1}^{M} \sqrt{P_i} \cos[2\pi(f_i - f_c)t + \theta_i] + n_s(t) \tag{C-3}$$

Combining the notation of Eq. (A-4) with the following parameters,

$$n_{cm} \equiv n_c\left(\frac{m}{W}\right) \qquad n_{sm} \equiv n_s\left(\frac{m}{W}\right)$$
$$\Delta_{ik} \equiv \frac{\pi}{W}\left(f_i - f_c - \frac{kW}{N}\right);\ |\Delta_{ik}| < \pi$$
$$C_{ik} \equiv \frac{1}{N}\sum_{m=0}^{N-1} \cos(2m\Delta_{ik})$$
$$D_{ik} \equiv \frac{1}{N}\sum_{m=0}^{N-1} \sin(2m\Delta_{ik}) \tag{C-4}$$
$$F_k \equiv \frac{1}{N}\sum_{m=0}^{N-1} (n_{cm} c_{km} - n_{sm} d_{km})$$
$$G_k \equiv \frac{1}{N}\sum_{m=0}^{N-1} (n_{cm} d_{km} + n_{sm} c_{km})$$

Eq. (A-7) reduces to

$$A_k = \sum_{i=1}^{M} \sqrt{P_i}\,(C_{ik}\sin\theta_i + D_{ik}\cos\theta_i) + F_k$$
$$B_k = \sum_{i=1}^{M} \sqrt{P_i}\,(C_{ik}\cos\theta_i - D_{ik}\sin\theta_i) + G_k \tag{C-5}$$

Consider the random variables F_k and G_k. Since $R_n(m/W) = 0$ for $m \neq 0$, the n_{cm}'s and n_{sm}'s are independent; they are also zero mean, jointly Gaussian random variables, with variance $R_n(0) = N_0 W/2$. Because F_k and G_k are linear combinations of the n_{cm}'s and n_{sm}'s, they are zero mean and jointly Gaussian. Furthermore,

$$\overline{F_k^2} = \frac{1}{N^2}\sum_{m=0}^{N-1}\sum_{n=0}^{N-1}\Big(\overbrace{\overline{n_{cm} n_{cn}}}^{\frac{N_0 W}{2}\delta_{mn}} c_{km} c_{kn} + \overbrace{\overline{n_{sm} n_{sn}}}^{\frac{N_0 W}{2}\delta_{mn}} d_{km} d_{kn} - \overbrace{\overline{n_{cm} n_{sn}}}^{0} c_{km} d_{kn} - \overbrace{\overline{n_{sm} n_{cn}}}^{0} d_{km} c_{kn}\Big)$$
$$= \frac{N_0 W}{2N^2}\sum_{m=0}^{N-1}\overbrace{\left(c_{km}^2 + d_{km}^2\right)}^{1} = \frac{N_0 W}{2N} \tag{C-6}$$

Similarly, we can show that

$$\overline{G_k^2} = \frac{N_0 W}{2N} \qquad \overline{F_k G_k} = 0 \tag{C-7}$$

so that F_k and G_k are independent and identically distributed.

Now conditioned on $\{P_i, f_i, \theta_i\}$, A_k and B_k are independent, jointly Gaussian random variables, with identical variances, but different, nonzero means in general. Therefore, the power spectral component S_k of Eq. (A-9) is conditionally a *noncentral* chi-square random variable with 2 degrees of freedom, and conditional mean

$$\overline{S}_k^{\,F_k, G_k} = \mu_k + \frac{N_0 W}{N} \tag{C-8}$$

where

$$\mu_k \equiv \sum_{i=1}^{M} \sum_{j=1}^{M} \sqrt{P_i P_j}\, [(C_{ik} C_{jk} + D_{ik} D_{jk}) \cos(\theta_i - \theta_j) + (C_{ik} D_{jk} - D_{ik} C_{jk}) \sin(\theta_i - \theta_j)] \tag{C-9}$$

Generally, the P_i's and f_i's are fixed but unknown parameters to be resolved by the spectrum analyzer. However, the θ_i's depend on the observation period, and can be regarded as independent, uniformly distributed random variables. So, while the mean spectral line power conditioned on $\{\theta_i\}$ contains cross terms (i.e., $i \neq j$ in Eq. C-9), the unconditional mean does not:

$$\overline{S}_k^{\,F_k, G_k,\ \{\theta_i\}} = \zeta_k + \frac{N_0 W}{N} \tag{C-10}$$

where

$$\zeta_k \equiv \overline{\mu_k}^{\,\{\phi_i\}} = \sum_{i=1}^{M} \sum_{j=1}^{M} \sqrt{P_i P_j}\, [(C_{ik} C_{jk} + D_{ik} D_{ik}) \overbrace{\cos(\theta_i - \theta_j)}^{\delta_{ij}} + (C_{ik} D_{jk} - D_{ik} C_{jk}) \overbrace{\sin(\theta_i - \theta_j)}^{0}]$$

$$= \sum_{i=1}^{M} P_i \left(C_{ik}^2 + D_{ik}^2\right) = \sum_{i=1}^{M} P_i \left(\frac{\sin N\Delta_{ik}}{N \sin \Delta_{ik}}\right)^2 \tag{C-11}$$

The last step in Eq. (C-11) follows from the series identifies (Ref. 6, p. 30)

$$C_{ik} = \frac{\sin N\Delta_{ik} \cos(N-1)\Delta_{ik}}{N \sin \Delta_{ik}}$$

$$D_{ik} = \frac{\sin N\Delta_{ik} \sin(N-1)\Delta_{ik}}{N \sin \Delta_{ik}} \tag{C-12}$$

We also note that the unconditional probability density function of S_k has the form (Ref. 5)

$$p(S_k) = \frac{N}{N_0 W} e^{-\frac{NS_k}{N_0 W}} e^{-\frac{N\mu_k}{N_0 W}} I_0\left(\frac{2N}{N_0 W}\sqrt{S_k \mu_k}\right) \tag{C-13}$$

which, in general, does not simplify to a noncentral chi-square distribution for $M > 1$.

As in Appendix B, we now extend our results to an L-look spectrum in which the k^{th} spectral component S_k^* is the average of L independent observations of S_k. Furthermore, we again use Eq. (B-13) to form the normalized discrete spectrum $\{v_k\}$. Let the phase of the i^{th} sinusoidal input component for the l^{th} look be denoted by θ_{il}. Conditioned on $\{\theta_{il}\}$, v_k is a noncentral chi-square random variable with $2L$ degrees of freedom: its conditional probability density function (Ref. 5) and mean can be expressed as

$$p(v_k \mid \{\phi_{il}\}) = L\left(\frac{v_k}{\lambda_k}\right)^{\frac{L-1}{2}} e^{-L(v_k+\lambda_k)} I_{L-1}(2L\sqrt{v_k \lambda_k})$$

$$\overline{v_k}^{\,\{\theta_{il}\}} = \lambda_k + 1 \tag{C-14}$$

where

$$\lambda_k \equiv \frac{N}{N_o W} \sum_{i=1}^{M} \sum_{j=1}^{M} \sqrt{P_i P_j}\, [(C_{ik} C_{jk} + D_{ik} D_{jk})\, \alpha_{ij} + (C_{ik} D_{jk} - D_{ik} C_{jk})\, \beta_{ij}] \tag{C-15}$$

and

$$\alpha_{ij} \equiv \frac{1}{L} \sum_{l=1}^{L} \cos(\theta_{il} - \theta_{jl})$$

$$\beta_{ij} \equiv \frac{1}{L} \sum_{l=1}^{L} \sin(\theta_{il} - \theta_{jl}) \qquad \text{(C-16)}$$

Since the θ_{il}'s are independent and uniformly distributed, for large L, we can approximate Eq. (C-16) by $\alpha_{ij} \cong \delta_{ij}$ and $\beta_{ij} \cong 0$: then

$$\lambda_k \cong \frac{N}{N_o W} \zeta_k = \sum_{i=1}^{M} \left(\frac{P_i N}{N_o W}\right) \left(\frac{\sin N\Delta_{ik}}{N \sin \Delta_{ik}}\right)^2 \qquad \text{(C-17)}$$

and we can essentially remove the conditioning restriction in Eq. (C-14). (Note that all of these approximations become exact for the special case $M = 1$.)

If a threshold detection approach is used, as in Appendix B, the false alarm probability is again given by Eq. (B-21). The probability of a miss on the k^{th} line must be computed by numerical integration techniques:

$$P_{M,k} \equiv Pr\,[v_k < \eta]$$

$$\cong \frac{L\, e^{-L\lambda_k}}{\lambda_k^{\frac{L-1}{2}}} \int_0^{\eta} dx\, x^{\frac{L-1}{2}} e^{-Lx} I_{L-1}^{(2L\sqrt{\lambda_k x})} \qquad \text{(C-18)}$$

For large L, the Bessel function can be accurately approximated by its asymptotic formula (Ref. 8, p. 378), simplifying the task of numerically evaluating Eq. (C-18):

$$P_{M,k} \cong \int_0^{\eta} dx\, e^{g_k(x)} \qquad \text{(C-19)}$$

where

$$g_k(x) \equiv ln\, L - \frac{1}{2} ln\,[2\pi (L-1) a_k(x)]$$

$$+ \left(\frac{L-1}{2}\right) ln \left(\frac{x}{\lambda_k}\right) + (L-1)\, b_k(x) - L(x + \lambda_k)$$

$$a_k(x) \equiv \sqrt{1 + \left(\frac{2L}{L-1}\right)^2 \lambda_k x}$$

$$b_k(x) \equiv a_k(x) + ln \left[\left(\frac{2L}{L-1}\right) \frac{\sqrt{\lambda_k x}}{1 + a_k(x)}\right] \qquad \text{(C-20)}$$

and λ_k is given by Eq. (C-17) in terms of the P_i's and f_i's (but independent of the θ_i's).

Appendix D

Aliasing Effects in DFT Power Spectrum

In Eq. (A-5), an integral over an infinite time interval is approximated by a finite sum of N samples of the integrand spaced $T/N = 1/W$ seconds apart. Although the spacing of the samples satisfies the Nyquist rate condition for the infinite-duration integrand (one-sided bandwidth $W/2$), the finite-time integrand has a larger bandwidth and requires a correspondingly higher sampling rate. Consequently, the DFT power spectrum typically exhibits frequency foldover and spectral spreading effects known as "aliasing."

To examine this effect more closely, consider a special case of Appendix C in which the input signal $x(t)$ is a single sinusoid with power P and frequency f_s, and neglect the additive noise. The one-sided power spectral density $S_x(f)$ consists of a single impulse of weight P at $f = f_s$, as shown in Fig. D-1a. Using the results in Appendix C with $M = 1$ and $N_0 = 0$, the DFT spectrum has envelope

$$E(f) = P\left[\frac{\sin\frac{N\pi}{W}(f - f_s)}{N\sin\frac{\pi}{W}(f - f_s)}\right]^2$$

$$\approx P\left[\frac{\sin\frac{N\pi}{W}(f - f_s)}{\frac{N\pi}{W}(f - f_s)}\right]^2 ; |f - f_s| << \frac{W}{2} \qquad \text{(D-1)}$$

and the k^{th} spectral line is simply

$$S_k = E\left(f_c + \frac{kW}{N}\right) \qquad \text{(D-2)}$$

The spectral spreading of the form $(\sin af/af)^2$ in Eq. (D-1) is a consequence of the flat T-second observation "window." Other windows can be used to reduce this effect (e.g., Ref. 2,3). Also, since $E(f)$ has period W, there is some foldover in the DFT spectrum when $|f_s - f_c|$ is near $W/2$. These aliasing effects are illustrated in Figs. D-1b and D-1c.

A special case is when $f_s - f_c$ is precisely equal to kW/N for some k, say $k = k_0$. Then Eqs. (D-1) and (D-2) yield

$$S_k = P\left[\frac{\sin\pi(k - k_0)}{N\sin\frac{\pi}{N}(k - k_0)}\right]^2 = P\,\delta_{kk_0} \qquad \text{(D-3)}$$

as illustrated in Fig. D-1d. So in this case only, the DFT spectrum looks like the actual spectrum of Fig. D-1a.

Note that for any choice of f_s, the total power in all of the DFT spectral lines is exactly P. Defining $\beta \equiv (\pi/W)(f_c - f_s)$, Eqs. (D-1) and (D-2) reduce to

$$S_k = P\left[\frac{\sin(N\beta + k\pi)}{N\sin\left(\beta + \frac{k\pi}{N}\right)}\right]^2 \qquad \text{(D-4)}$$

from which it follows that

$$\sum_{k=-\frac{N}{2}}^{\frac{N}{2}-1} S_k = \frac{P}{N^2}\sin^2 N\beta \underbrace{\sum_{k=-\frac{N}{2}}^{\frac{N}{2}-1} \sin^{-2}\left(\beta + \frac{k\pi}{N}\right)}_{\frac{N^2}{\sin^2 N\beta}\ \text{(Ref. 9)}} = P \qquad \text{(D-5)}$$

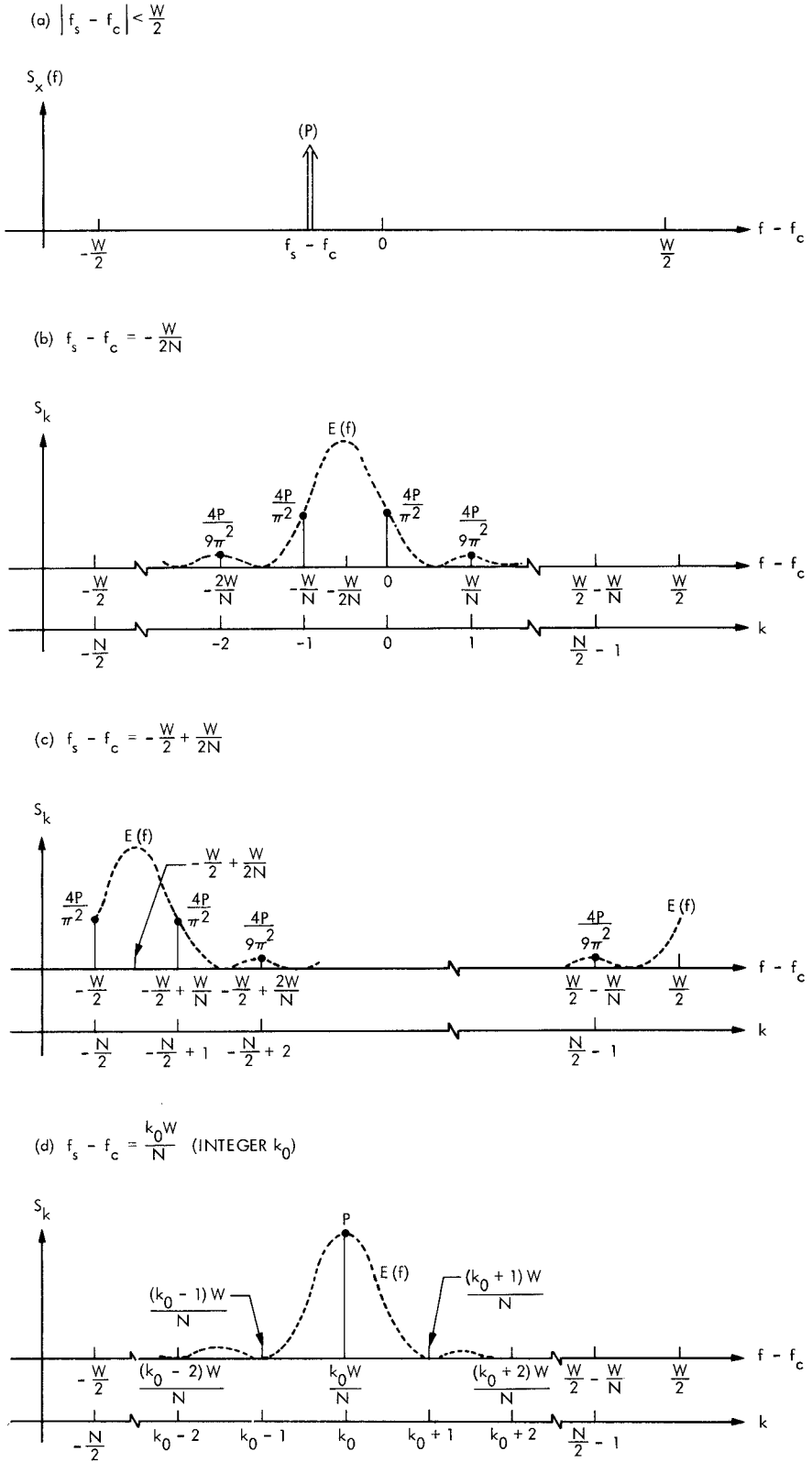

Fig. D-1. Comparison of one-sided power spectral density $S_x(f)$ of sinusoidal carrier with power P at frequency f_s and DFT spectral lines $\{S_k\}$ at frequencies kW/N

References

1. Levitt, B. K., "Radio Frequency Interference from Near-Earth Satellites," in *The Deep Space Network Progress Report 42-37,* Jet Propulsion Laboratory, Pasadena, Calif., Feb. 15, 1977.

2. Oppenheim, A. V., and Schafer, R. W., *Digital Signal Processing,* Prentice-Hall, Englewood Cliffs, New Jersey, pp. 549-553, 1975.

3. Welch, P. D., "The Use of Fast Fourier Transform for the Estimation of Power Spectra: A Method Based on Time Averaging over Short, Modified Periodograms," *IEEE Trans. Audio Electroacoust.,* Vol. AU-15, pp. 70-73, June 1967.

4. Wozencraft, J. M., and Jacobs, I. M., *Principles of Communication Engineering,* John Wiley, New York, New York, 1965.

5. Miller, K. S., *Multidimensional Gaussian Distributions,* John Wiley, New York, New York, p. 56, 1964.

6. Gradshteyn, I. S., and Ryzhik, I. M., *Table of Integrals, Series, and Products,* Academic Press, New York, New York, 1965.

7. Van Trees, H. L., *Detection, Estimation, and Modulation Theory, Part I,* John Wiley, New York, New York, p. 110, 1968.

8. *Handbook of Mathematical Functions,* U.S. Govt. Printing Office, M. Abramowitz and I. A. Stegun, ed., Washington, D.C., 1964.

9. Jolley, L. B. W., *Summation of Series,* Dover Publications, New York, New York, pp. 92-93, 1961.